Impulse Measurements of Electric Solid Propellant in an Electrothermal Ablation-Fed Pulsed Plasma Thruster

Matthew S. Glascock,[1]
Missouri University of Science and Technology, Rolla, Missouri, 65409, USA

Joshua L. Rovey,[2]
University of Illinois Urbana-Champaign, Urbana, Illinois, 61801, USA

and
Kurt A. Polzin[3]
NASA Marshall Space Flight Center, Huntsville, Alabama, 35812, USA

Electric solid propellants are advanced solid chemical rocket propellants that can be controlled (ignited, throttled and extinguished) through the application and removal of an electric current. These propellants are also being considered for use in the ablative pulsed plasma thruster. In this paper, the performance of an electric solid propellant operating in an electrothermal ablation-fed pulsed plasma thruster was investigated using an inverted pendulum micro-Newton thrust stand. The impulse bit and specific impulse of the device using the electric solid propellant were measured for short-duration test runs of 100 pulses and longer-duration runs to end-of-life, at energy levels of 5, 10, 15 and 20 J. Also, the device was operated using the current state-of-the-art ablation-fed pulsed plasma thruster propellant, polytetrafluoroethylene or PTFE. Impulse bit measurements for PTFE indicate 100±20 μN-s at an initial energy level of 5 J, which increases linearly by ~30 μN-s/J with increased initial energy. Measurements of the impulse bit for the electric solid propellant are on average lower than PTFE by 10% or less. Specific impulse for when operating on PTFE is calculated to be about 450 s compared to 225 s for the electric solid propellant. The 50% reduction in specific impulse is due to increased mass ablated during operation with the electric solid propellant relative to PTFE.

I. Introduction

Recent innovations in the solid rocket propellant field have led to the development of a solid propellant that is safe, throttleable, and green with on-demand on-off capability. These electric solid propellants (ESP's) ignite and decompose when electric power is applied at sufficient current and voltage [1]. This decomposition is a highly exothermic process that generates hot gas at a burn rate that can be throttled by varying the applied current. Removal of the voltage and current extinguishes the reaction, which may be restarted by reapplication of electric power [2]. Because this reaction is only induced by electric current, ESPs are not susceptible to accidental ignition by spark, impact or open flame. These characteristics are extremely beneficial compared to traditional solid rocket propellants which are not throttleable, toggleable, or insensitive to external ignition sources. The advent of ESPs expands the potential applications for solid propellants that were previously infeasible.

Development of ESPs began in the 1990's with the design of an automobile air bag inflator propellant (ABIP) using materials safe for unprotected human contact (i.e., "green" materials). This ABIP was ammonium nitrate-based and was later repurposed for use in other areas, including rocket propulsion. Shortly thereafter, "ASPEN," the first digitally controlled extinguishable solid propellant, was developed [3]. This propellant featured additives with the ammonium nitrate base to lower melting point and increase electrical conductivity [2]. This material exhibited performance metrics comparable to that of previous solid rocket propellants, but major problems existed with the repeatability of ignition. Further development for gas-generation applications led to a special family of electrically

[1] Graduate Research Assistant, Aerospace Plasma Lab, 160 Toomey Hall, 400 W. 13th St, AIAA Student Member.
[2] Associate Professor of Aerospace Engineering, 317 Talbot Lab, 104 S. Wright St, AIAA Associate Fellow.
[3] Space Systems Team Lead, Advanced Concepts Office, 4221 Rideout Rd., AIAA Associate Fellow.

controlled energetic materials which may be mixed as either solid, liquid or gel form propellants, all of which are electrically ignitable [4, 5]. Some mixtures are flame-sensitive and explosive, some insensitive to flame and sustainable, some are insensitive and extinguishable (like ESPs). One particular formula which conducts electricity and exhibits high specific impulse is known as the high performance electric propellant, or HIPEP [1, 6], which is not sensitive to open flame, spark, or impact and is extinguishable. In this solid energetic material, the ionic liquid oxidizer hydroxyl-ammonium nitrate (HAN) is dissolved and cross-linked in polyvinyl alcohol (PVA), forming a gel that is hardened by baking. The resulting rubbery solid HIPEP exhibits a pyroelectric behavior unique to energetics. When direct current electric power is applied, the proton transfer reaction between hydroxyl-ammonium and nitrate is promoted, and the level of nitric acid rapidly rises in the material eventually triggering ignition of the propellant. This exothermic, gas-generating reaction may be harnessed in a solid rocket motor to generate thrust on demand using electric power.

HIPEP's pyroelectric behavior may facilitate a dual mode propulsion system using the solid propellant. The first mode is a high thrust chemical mode where direct current electric power is applied to incite pyroelectric gas generation. This propellant is gas-dynamically accelerated through a nozzle to generate thrust like any typical solid rocket motor. The duration of each chemical mode fire is determined by the duration that electric power is supplied and could be ~500 ms. The inventors of this propellant and collaborating groups have reported on this mode of operation previously, with some ongoing efforts [7-9]. This solid rocket motor may be paired with a second, high specific impulse (I_{sp}) electric mode in the same device using the same thruster and solid propellant with a second electrical circuit configuration. One promising electric configuration for a high I_{sp} mode is a pulsed electric propulsion device known as the coaxial ablation-fed pulsed plasma thruster (APPT).

Pulsed plasma thrusters [10] (PPTs) have been in use since the first orbital flight of an electric propulsion device in 1964. PPTs offer repeatable impulse bits with higher exhaust velocities than can be achieved using chemical thrusters. Ablating polytetrafluoroethylene (PTFE) in a discharge to yield a working fluid, APPT's have the added benefit of inert propellant storage with no pressure vessel requirements. PPT's typically fulfill secondary propulsion needs on spacecraft such as station-keeping and attitude control, but have recently garnered more attention as main propulsion for small spacecraft [11, 12]. Broadly, APPT's may be classified as either rectangular or coaxial geometry [10]. Coaxial geometry APPTs, like that of the PPT-4 [13], electrothermal PPTs [14-18], or ablative z-pinch PPTs [19], begin with a central and a downstream electrode and may have a conical-shaped dielectric between the electrodes. The central or upstream electrode is typically cylindrical and positively charged (anode) while the downstream electrode is ring-shaped. Solid propellant fills the space between electrodes and may be fed from the side through the conical dielectric. Most commonly this propellant is the inert polymer, PTFE, which is the state-of-the-art propellant for APPTs. A capacitor or bank of capacitors is charged to a few kilovolts, with that voltage applied across the electrodes. The main arc discharge is initiated by an igniter, which is always located in or near the cathode in a PPT. The igniter generates a surface flashover discharge to create a seed plasma, initiating the main arc discharge. Radiation from this high temperature arc discharge heats the surface of the solid propellant, yielding gaseous propellant through ablation, which further fuels the arc. The coaxial PPT is a device dominated by electrothermal acceleration mechanisms, with the energy of the arc heating the gas to yield high exit velocities through gas-dynamic acceleration. Ablation processes are at the core of APPT operation, with many PTFE ablation studies in the literature [20-25].

The aforementioned dual mode device combining a solid chemical rocket motor mode with an electric coaxial APPT mode remains conceptual. Research in the use of HIPEP and other ESPs for gas-generation and chemical mode applications with long (>1 ms) timescales is ongoing and separate from the present work. Current efforts by the authors are focused on understanding the behavior of the HIPEP material in the proposed APPT pulsed electric mode. Our recent work has compared ablation of HIPEP with traditional PTFE in ablation-fed arc discharge devices [26-28]. At high temperatures and over long (~ms) time-scales, it is known that HIPEP undergoes a thermal decomposition process, while PTFE evaporates after depolymerization. However, ablation-controlled arc discharges occur on much shorter timescales, as the discharge current has a period of less than 10 μs. The specific ablation (μg/J) of HIPEP was measured to be roughly twice that of PTFE, and this difference was attributed to differences in the material thermal and chemical properties [26]. Plume measurements of HIPEP-fueled pulsed microthrusters [27] indicate electron temperatures (1-2 eV) and densities (10^{11}-10^{14} cm^{-3}) of the weakly ionized plasma comparable to that of PTFE fueled APPTs. Exhaust velocity measurements indicate similar performance of HIPEP relative to PTFE in the microthrusters. Further, it has been shown that the fraction of late-time ablation mass is similar for both propellants. Estimates from high-speed imagery of a pulsed HIPEP microthruster suggest that up to 50% of the ablated mass may be attributed to low-speed macroparticles ejected after the main current pulse [28].

To date, HIPEP has not been used in a traditional APPT configuration, where propellant material is ablated during a high current, short duration (~10 μs) arc discharge. Another ESP, the ammonium nitrate-based ABIP, was previously tested in Aerojet's modular test unit (MTU) and reported impulse bits were roughly 50-80% of the

polytetrafluoroethylene (PTFE) solid propellant typically used in this unit [1]. No performance (impulse/thrust, specific impulse) metrics are yet published for a PPT using HIPEP as propellant. The objective of this work is to investigate the performance of the HAN-based HIPEP material relative to that of PTFE in an electrothermal APPT. The device is a coaxial geometry electrothermal APPT and a modified version of it was used previously to quantify the propellant specific ablation [26]. Both PTFE and HIPEP are used as propellants in this work and the impulse bit and specific impulse are measured using an inverted pendulum thrust stand. For each propellant, the device was operated for 100 or more pulses in vacuum, with the impulse bit measured throughout the test and the average propellant mass loss per pulse found by massing the propellant before and after a test. These measurements are the first reported one-to-one performance comparisons between the HIPEP and PTFE materials in an ablative pulsed plasma device. Results from these experiments, when combined with previous observations on the ablation of the HIPEP material, can now be correlated to draw conclusions about the propulsive performance.

II. Experimental Methods and Apparatus

We begin with a discussion of the methods and equipment used in the test trials in this work. First, details on the chemical composition and behavior of the HIPEP material are discussed. Next, we describe the geometry and basic operation of the electrothermal APPT device. Finally, a description of the thrust stand and associated calibration and data collection methods are reviewed.

A. High Performance Electric Propellant

HIPEP is a HAN-based solution solid manufactured by Digital Solid State Propulsion (DSSP) using "green" ingredients and processes free of harmful fumes. HIPEP has a chemical composition of 75% HAN oxidizer (an inorganic ionic liquid), 20% polyvinyl alcohol (PVA) fuel binder, and 5% ammonium nitrate. It is mixed in standard chemical glassware, with only gloves and safety glasses needed for protection, and cured at 35°C/95°F. It is initially a liquid and poured into a mold, curing to form a rubbery solid with density ~1.8 g/cm^3 and the appearance and texture of a soft pencil eraser. In a typical PPT, the PTFE is an electrical insulator between the electrodes. The conductivity of HIPEP (1-2 S/m) is comparable to highly conductive ionic liquids. However, our previous work has shown that the conductivity of the HIPEP has a negligible effect on the measured current in the arc discharge. Further, it has been observed that the HIPEP material ablates more readily than PTFE in an ablation-fed arc, which may be attributed to thermodynamic properties of the solid propellant. It is currently unclear how the additional ablation mass contributes to the thrust produced by the material in an ablation-fed thruster.

The solid HIPEP material is hygroscopic and gradually absorbs moisture from a typical laboratory atmosphere (~50% rel. hum.), eventually causing the propellant to become completely liquid. To mitigate absorption of moisture in this work, HIPEP samples are handled and measured only in a dry-air glovebox kept at 5% relative humidity. Further, these samples undergo a vacuum drying process wherein samples were kept at $<5\times10^{-2}$ torr for at least 24 h. After this time, samples have reached steady state and the measured mass is within 0.26% of the dry mass [26].

B. Electric Propellant Thruster Experiment

The electric propellant thruster experiment (EPTX) has geometry similar to that of a coaxial electrothermal APPT. Figure 1 details the geometry of the device. It should be noted that this device was originally used primarily to study the mass ablation of the propellants and not as a thruster [26]. The device was designed to facilitate removal and replacement of small propellant tube samples and is not optimized for performance. A circular stainless steel rod serves as the anode (positive) and a stainless steel ring with a 15° conical nozzle bore serves as the cathode (ground). The assembly is housed in a nonconductive PEEK body. The propellant tube sample has length 12 mm and inner diameter 6.35 mm. Because HIPEP is conductive, the propellant is isolated electrically from the two electrodes by thin PTFE washers with inner diameter ~7 mm which are not shown in Figure 1. These washers have an approximate thickness of <0.5 mm which is sufficient to hold off the maximum voltage (2.23 kV) used in the present work. The washers remain during PTFE testing to keep electrode spacing consistent between propellant samples. The test article and the capacitor bank are co-located inside the vacuum test facility. It is intended that the arc discharge occurs in the cylindrical cavity (6.35 mm dia.) formed by the inner propellant tube wall and the anode end. Because the test article is at vacuum, the capacitor can be charged to a high voltage (1-5 kV) across the anode/cathode-gap without initiating a Paschen breakdown. Breakdown of the gas is initiated by a surface discharge igniter constructed of two tungsten wires cemented in a two-bore alumina tube with ~2 mm exposed tip lengths. The wire tips are embedded in the nozzle of the cathode as shown in Figure 1. A capacitor discharge ignition (CDI) circuit creates a low energy surface discharge between the tungsten wire tips. Electrons from this discharge are accelerated to the positively charged anode and sputter particles from it and the nearby propellant, triggering the main arc discharge.

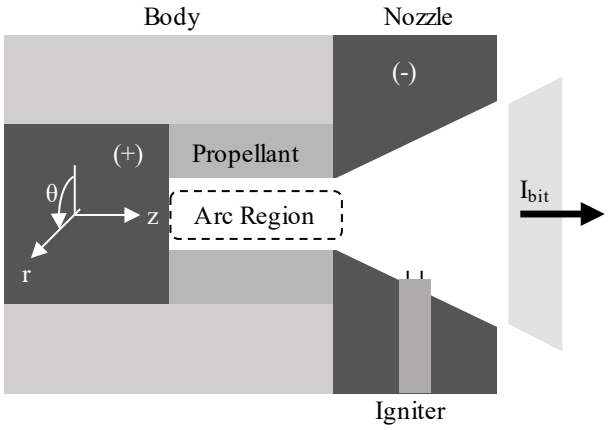

Figure 1: Diagram of the electric propellant thruster experiment.

During the main arc discharge current flows in the z-direction through the arc region from the anode and attaches at the cathode/nozzle electrode. This current oscillates between high positive and negative currents over a few microseconds. Because the magnetic field induced by this rapidly changing current is in the θ-direction and follows the sign of the current, the Lorentz force is always directed in the negative radial direction (pinching toward the *z*-axis) in the arc region labeled in Figure 1. Thus, the current sheet does not propagate along the *z*-axis in the cavity. In the conical nozzle region there is a radial component of current that may give rise to a small electromagnetic thrust component. The high current flowing through the resistance of the arc discharge in the cavity dissipates the energy that was initially stored on the capacitors. This energy transiently heats the walls of the propellant cavity to well above the vaporization temperature and causes ablation of propellant mass of ~30-300 μg/pulse. The gas generated by ablation is then further heated by the arc discharge to high temperatures on the order of a few eV. This mass of high temperature charged particles and neutrals are accelerated gas-dynamically via the nozzle and impart an impulse per pulse or impulse bit (I_{bit}). The capacitor bank must be recharged after each discharge and is triggered again at a repetition rate of once per ~20 seconds in this work. This low repetition rate means the propellant cools to room temperature after each discharge. Further details on operation, propellant sample preparation, and the ablation mass of PTFE and HIPEP in the precursor to this device may be found in our previous publication [26]. The only change in the device between that work and the present work is the change to a conical nozzle shape cathode.

C. Compact Thrust Stand

This work was conducted in Electric Propulsion Facility 1 at the University of Illinois Electric Propulsion Lab. This vacuum facility is approximately 1000 L in volume and achieves a nominal base pressure of ~2×10^{-5} torr. Housed in this facility is the UIUC Compact Thrust Stand designed for accurate measurement of thrust and impulse bit in the micro- and milli-Newton range [29]. This stand is of an inverted-pendulum design as shown in Figure 2 with a footprint of only 20x39 cm and 50 kg thruster mass capacity. Two modes of stand operation allow for constant thrust force measurement in the range of 1-10 mN and impulse bit measurement in the range of 0.1-3 mN-s. In this work, the stand is operated in impulsive measurement mode to determine the impulse bit of the electrothermal APPT device. In Figure 2, the thruster and hardware are mounted on top of the long stand platform which is mounted to the fixed frame by stainless steel arms with torsional flexures. These flexures allow the stand to stabilize at a neutral position with completely vertical arms which would otherwise be an unstable position. Further, any motion of the stand platform in the x-direction causes deflection of the stand arms and is opposed by the spring force of the torsional flexures. This assembly allows for oscillatory motion of the stand platform in the x-direction about the neutral position. Thrust stand calibration is performed using a method similar to the one described in Polk, *et al*. [30] for impulsive measurement using an inverted-pendulum thrust stand. A small impact hammer constructed of aluminum body and soft plastic head is mounted to a hinge and actuated by a solenoid. The solenoid is triggered remotely with a circuit that includes a potentiometer allowing for adjustment of plunger speed. When triggered, the head of the hammer strikes the center of a piezoelectric force transducer at the impact location shown in Figure 2. This strike delivers an impulsive force to the stand platform and generates motion in the x-direction. The output signal from the transducer is delivered to an oscilloscope providing a measurement of the force imparted over time. The impulse delivered to the stand may be calculated by integration of the transducer signal. In this work, the hammer delivers a calibration impulse bit in the range of roughly 100-1400 μN-s, with adjustment in this range facilitated by remote adjustment of the potentiometer.

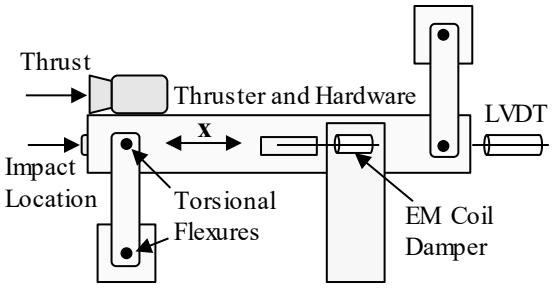

Figure 2: Diagram of the inverted-pendulum design UIUC Compact Thrust Stand.

For each strike of the hammer, the voltage waveform output by the force transducer is saved via the oscilloscope and later converted to force and integrated numerically. The measurement error for each hammer strike is ±6 μN-s due to bit noise and trapezoidal integration error. The motion of the thrust stand is monitored over time by a linear variable differential transformer (LVDT) affixed to the rear of the stand platform. This device outputs an analog voltage signal indicating the linear position of the stand platform that is digitized and monitored by a lab computer. Typical noise levels for this analog signal are on the order of 10^{-4} V, peak-to-peak. The output of the LVDT is used in two important ways during thrust stand operation. First, the digitized output is differentiated and fed through an amplifier to the electro-magnetic coil damper affixed between the stand platform and the fixed frame. This circuit uses magnetic eddy currents which increase in strength with voltage and interact with a metal shaft to retard movement of the stand platform towards zero velocity. Second, the output is logged to a file every 125 ms and later processed numerically to determine the response of the stand to an applied impulse bit. Specifically, the differential between successive position measurements (i.e., the velocity of the stand platform) is examined. For each strike of the impact hammer during calibration, a distinct peak in the differential voltage waveform is detected. The value of this peak in Volts is known as the response of the stand to the applied impulse bit.

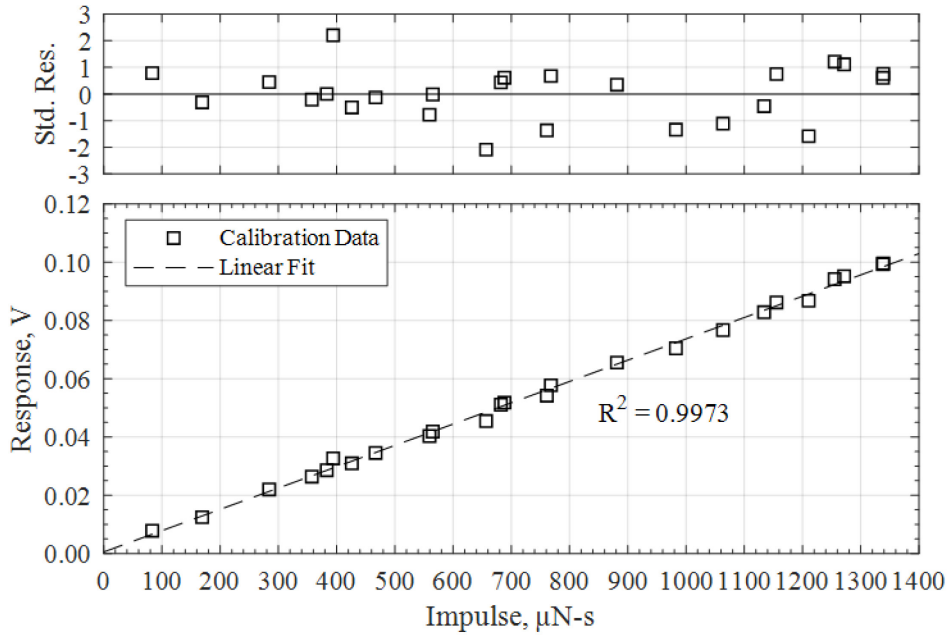

Figure 3: Typical pre-test thrust stand response calibration data as a function of applied impulse bit (bottom) and corresponding standardized residuals for the response data (top).

In this work, calibration was performed immediately prior to and following each testing session. Typically, 20-25 impulsive pulses are delivered to the stand and both transducer and LVDT output signals stored to memory for each. The response of the stand is plotted on the *y*-axis, the applied calibration impulse bits are plotted on the *x*-axis, and a linear fit to the data is established as the calibration curve. Figure 3 presents such a calibration curve for a typical pre-test calibration in the range of ~100-1400 μN-s. A standard least-squares regression method as described in Polk, *et al.*, [30] is used to determine the best linear fit to the calibration data. Also shown in Figure 3 are the standard residuals

shown relative to the average standard residual indicated by the solid black line. A standard residual is the difference between the *y*-value predicted by the linear fit and the value measured in calibration (the residual) normalized by the standard deviation of the residuals. Standard residuals falling uniformly between -2 and +2 and randomly distributed around zero are indicative of a correctly assumed form of fit for the calibration curve. In Figure 3, the mean standard residual is $<10^{-12}$, which is typical in this work, and indicated by the solid black line. The value of the square of the correlation coefficient, or R^2, indicates the percentage of variation captured by the fit, and typical values for this work are 0.95 or greater, as indicated in Figure 3. After each calibration, a testing session was conducted wherein the EPTX device was pulsed once every ~20 seconds, imparting an impulse on the stand. For each pulse of the device, the thrust stand response was obtained from the LVDT measurement. The calibration curve in Figure 3 was then used to determine the impulse bit of each pulse based upon the measured thrust stand response. In the present work, the impulse bits measured are in the range of roughly 100-800 μN-s, which is fully contained in the linear region of the established calibration curve. A typical standard deviation of residuals in calibration is 1.5 mV. Using the linear fit in Figure 3, this suggests the error in a single impulse bit measurement is ±20 μN-s, equivalent to one standard deviation of response residual in either direction.

III. Results

The EPTX was operated in the facility described and tested using PTFE and HIPEP as propellants for comparative purposes. Using the compact thrust stand, the impulse bit of each propellant was recorded for four nominal stored energy values of 5, 10, 15, and 20 J. Two test durations were conducted in this work: a short-duration test consisting of 100 pulses and a long-duration test to end-of-life. In this section, we present the results of these tests. First, short-duration test results are presented for each propellant operating at a single initial energy value, and then the average impulse bit over the short-duration tests at each energy level for both propellants are presented. Finally, the trend of impulse bit over the long-duration tests and the average impulse bit-per-joule of initial stored energy over the test duration is presented.

A. Short-Duration Tests

In our previous work, PTFE and HIPEP were tested in a similar device specifically designed to quantify the ablated mass per pulse [26]. The nominal test duration for that work was 100 pulses, which was initially selected as the test length for the short-duration test in this work. Each test begins with a ~20 point calibration at the nominal base pressure of 2×10^{-5} torr. The high voltage power supply is then set to the voltage corresponding to the desired energy level and impulse testing begins. Each pulse is triggered remotely via a surface discharge igniter and imparts an impulse to the thrust stand which is recorded and post processed to yield the impulse bit by the method described in section II.C. Figure 4 presents results from short-duration tests subdivided for each energy level. Six separate 100 pulse test trials are shown at each energy level, three for PTFE and three for HIPEP. The estimated error for a single impulse bit measurement (±20 μN-s) is shown by black error bars.

It is observed in the Figure 4b 10 J measurements that the impulse bit between pulses 10-100 varies in the range of 250-300 μN-s for both propellants. However, it is noted that the measured impulse bit for the first pulses of all six trials is >350 μN-s which is 30% greater than the average impulse bit. Subsequent pulses 2-10 decrease in all trials until a rough steady state is achieved in the 250-300 μN-s range. This phenomenon of initially high and then decreasing impulse bits as the propellant surface is conditioned over the first few pulses has previously been observed in the literature [16, 19]. The impulse bit then varies about the mean and remains roughly constant, within the error bars, through pulse 100. The average impulse bit for all 3 tests (300 total pulses) shown for PTFE at the 10 J energy level is 278 μN-s, and for HIPEP is 271 μN-s. The standard deviation for all measurements in Figure 4b is ~22 μN-s. This is largely attributed to the measurement error resulting from the variation of stand response around the linear calibration curve. For each other energy level (5, 15, 20 J), three separate test trials were performed for each propellant and are shown in Figure 4a c, and d, respectively. This yields 24 one-hundred pulses trials, 12 trials for each propellant. All of these trials yielded impulse bit measurement results of the same form as Figure 4b, except one, Figure 4d, HIPEP-20-2. That is, all 23 of 24 trials show a first impulse bit measurement >30% above the average, decreasing between pulses 2-10, and variation around the mean with a constant trend for pulses 10-100. Further, all six trials at each energy level show similar mean values. The only major difference in results for other energy levels are the magnitude of the impulse bit measurements, which are shifted proportionally and discretely with energy level. HIPEP-20-2 shown in Figure 4d exhibited differing and unique behavior. In this trial, the impulse bit for pulses 1-10 were near the mean value of 608 μN-s, rather than 30% greater. An increasing trend over pulses 10-40 is observed, peaking at a value of ~700 μN-s, before decreasing again to end near the mean of the other trials. While this trial

deviated significantly from the typical trend observed in the other subfigures of Figure 4, the mean impulse bit of this trial is still similar to the other five trials at 20 J.

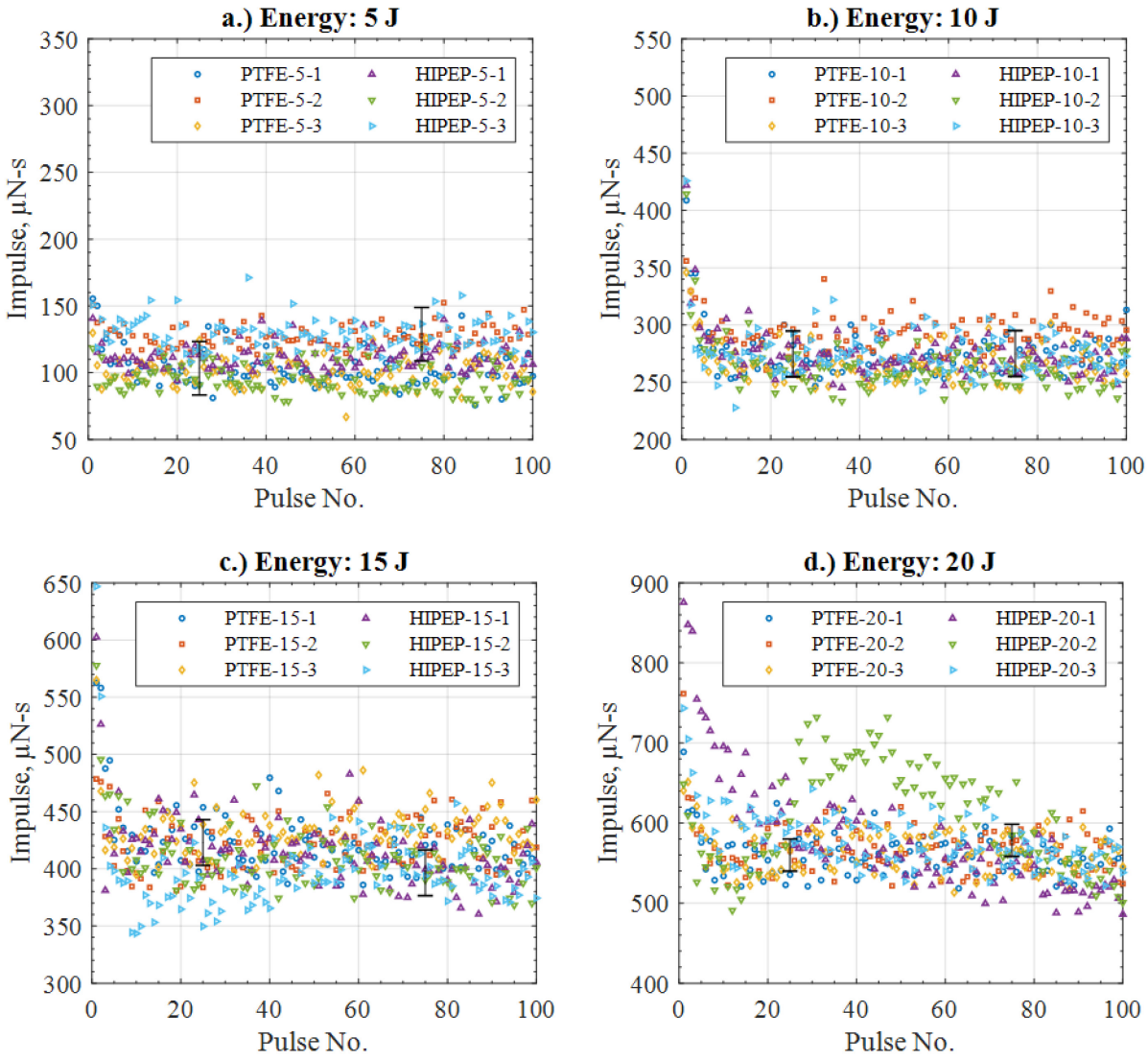

Figure 4: Impulse bit measurements for short-duration tests with both propellants and for a.) 5 J, b.) 10 J, c.) 15 J, and d.) 20 J nominal initial energy. Note the *y*-axis scales are adjusted for each plot.

Figure 5 presents the impulse bits averaged over 300 pulses (3 propellant samples at 100 pulses each) at each energy level for each propellant, with error bars indicating two standard deviations above and below the average. Also shown in Figure 5 is a linear fit and coefficients to the results for both propellants. From the average impulse bit results in Figure 5, it is observed that impulse bit increases linearly with initially stored energy with a slope of ~30 μN-s/J for both propellants. Impulse bit values at each energy level are nearly identical between propellants. At the 20 J energy level, HIPEP exhibits an average impulse bit of 590 μN-s compared to 565 μN-s for PTFE, a difference of 25 μN-s, or about 5%. This is the largest discrepancy between propellants at any energy, and 20 J is the only energy level where a larger impulse bit is measured for HIPEP. Standard deviation in impulse bit also increases with energy level for both propellants, but not at the same rate. The standard deviation for PTFE has a value of 16 μN-s at 5 J and 29 μN-s at 20 J, with a roughly linear slope between the two. At 5 J, HIPEP impulse bit standard deviation is 17 μN-s, similar to PTFE, but increases to 62 μN-s at the 20 J level. The standard deviation for HIPEP at 20 J was largely affected by the one anomalous short-duration trial previously discussed (see Figure 4d HIPEP-20-2). As a result of this trial's unique trend, the standard deviation for HIPEP measurements at 20 J is significantly increased compared

to other energy levels and PTFE. Otherwise, the mean impulse bit at a given energy for HIPEP is typically ~95% of the mean impulse bit for PTFE, with increased variation (~10% larger standard deviation) about the mean.

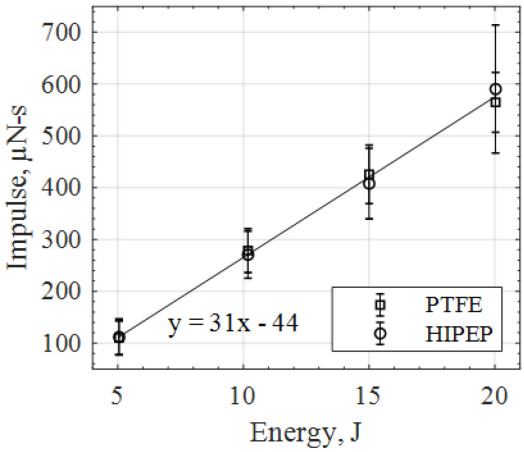

Figure 5: Average impulse bit over all short-duration tests at each initial energy for each propellant (error bars are a 2-σ standard deviation).

B. Long-Duration Tests

Also of interest in the present work is the trend of impulse bit over the entire lifetime of a propellant sample. Long-duration test trials were conducted using the same EPTX device and both HIPEP and PTFE propellant samples. In these trials, the device is pulsed at the same repetition rate, and impulse bit measured using the compact thrust stand as in the short-duration trials, but over a greater time period (>24 h). Automated pulsing of the EPTX device is achieved by use of a battery-powered timer circuit which remotely triggers the surface discharge igniter once every 22 seconds. At beginning of life, the inner diameter of a propellant sample is at the nominal dimension (6.35 mm) and the main arc discharge is easily triggered by the igniter. Each discharge ablates propellant material from the inner wall of the sample and gradually increases the diameter of the cavity in which the arc forms. As this diameter increases, ignition of the arc discharge becomes more difficult, and the time between successive pulses increases to two or more multiples of 22 s. That is, the first trigger event may not initiate arc formation, and a second or third trigger event is required. End-of-test in this work is defined as the pulse number where the time between pulses is in excess of 1 h, which means 160 trigger events do not initiate arc formation. The long-duration test trials begin with fresh samples of nominal inner diameter and end at the sample end-of-life as just previously defined. Figure 6 presents the measurements of impulse bit over these long duration tests for the four nominal energy levels and for each propellant. Error bars here show the estimated measurement error for a single impulse bit measurement (±20 µN-s).

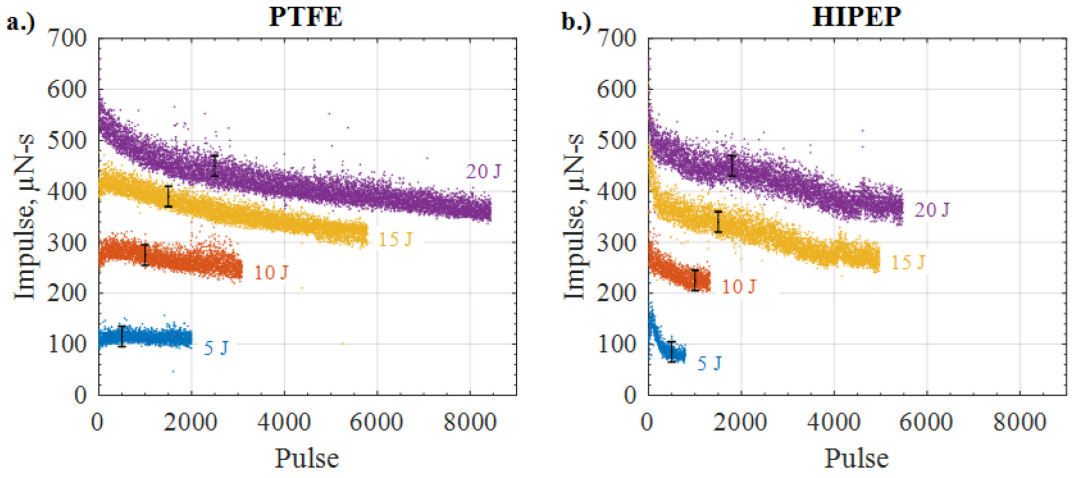

Figure 6: Impulse measurements for long-duration tests with a.) PTFE and b.) HIPEP propellant.

In Figure 6, it should first be noted that for each long-duration trial, comparison of pulses 1-100 shows close agreement with the trends observed in short-duration testing (Figure 4). For example, pulse 1 at 5 J using PTFE was measured to produce 130 μN-s and the impulse bit decreased to a mean value of about 115 μN-s over the first 100 pulses. Beyond pulse 100, PTFE impulse bit measurements at 5 J in Figure 6a are largely constant, and the mean over the full lifetime is 114 μN-s. At increased discharge energy, over the duration of the test a decreasing trend in impulse bit is observed. At 10 J, PTFE impulse bit measurements average ~274 μN-s through 100 pulses, but ~268 μN-s at end-of-life (3,083 pulses). A rough linear fit indicates the impulse bit decreases by about 1.1 μN-s per 100 pulses for PTFE at 10 J. At 15 J, this decrease is slightly greater in magnitude (1.8 μN-s per 100 pulses) but still nearly linear, and the average over the 5,783 pulses is 361 μN-s. At 20 J, the average over the full 8,445 pulses is 418 μN-s and a decreasing trend is still observed, but the profile deviates from a linear shape. Further, it is noted in Figure 6a that the lifetime of the test trial increases with energy level. Lifetime for PTFE is 8,445 pulses at 20 J compared to 2,000 pulses at 5 J. In Figure 6b for HIPEP testing, a similar trend of increasing lifetime with discharge energy is observed for HIPEP. This increase is most apparent between the 10 and 15 J energy levels, where pulse lifetime increases from 1,323 to 4,974 pulses. From beginning to end-of-life, however, slightly different trends are observed for HIPEP compared to PTFE. At 5 J, the decrease in impulse bit for HIPEP is much greater than for PTFE, decreasing by 19 μN-s per 100 pulses. Average impulse bit through pulse 100 is 120 μN-s but a decreasing trend is observed through the final pulse, and the lifetime is much shorter than 5 J for PTFE (793 vs. 2,000 pulses). These comparison trends continue at the higher energy levels, with HIPEP impulse bit typically decreasing more than PTFE over a shorter lifetime at a given energy. More discussion on the comparison of PTFE and HIPEP sample lifetimes may be found in Section IV.B.

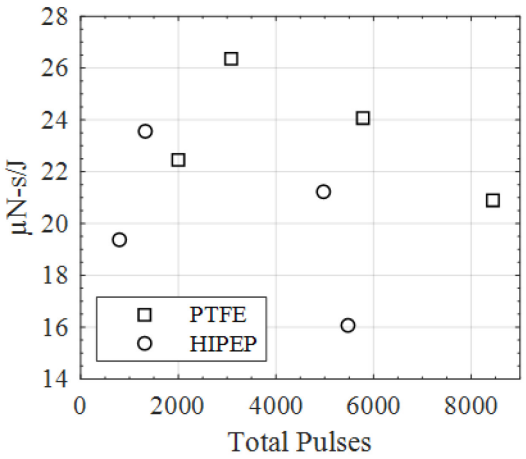

Figure 7: Average impulse bit per joule from the long-duration testing plotted as a function of total pulses.

Figure 7 presents the average impulse bit-per-Joule at end-of-life as a function of total pulses. Each point corresponds to the mean values for each test trial shown in Figure 6 over the full length of each test individually. For both propellants, the leftmost point (shortest lifetime) corresponds to the 5 J energy level trial, and the longest lifetime is for the 20 J energy level, as noted in Figure 6. Apart from the shortest lifetime points, both propellants generally exhibit a decrease in average impulse bit-per-Joule with lifetime. The short lifetime (low energy) point is noticeably decreased compared to the subsequent trend of the other points. This observation is combined with another to indicate a unique mode of operation for the low energy level in section IV.A. Excluding the first data points in each series of Fig. 7, PTFE exhibits an approximately linear decrease in impulse bit per Joule of ~1 μN-s/J per 1000 pulses. Due to the limited test duration for HIPEP at 20 J compared to PTFE at similar energy, the corresponding points for HIPEP do not appear to follow the same linear trend as PTFE. Figure 7 highlights the previous observations on impulse bit and lifetime of HIPEP compared to PTFE. HIPEP impulse bits are typically about 90-99% of the value measured for PTFE for a given initial energy, resulting in a 10% reduction in the HIPEP data. Also, at each discharge energy the lifetime for the HIPEP samples is up to 60% less than PTFE.

IV. Analysis and Discussion

Further details and discussion concerning the results presented in the previous section are provided here. We begin with a brief discussion of the mass loss during testing and the resulting specific impulse for each propellant.

Discussion of the observed difference in lifetime of the two propellants in the EPTX device configuration follow. Comparison of these key metrics between the two propellants are a focus in this section.

A. Specific Impulse

One of the most commonly reported performance metrics for in-space propulsion devices is the specific impulse, or I_{sp}. This quantity is expressed in seconds and describes the efficiency at which the device can generate thrust per unit mass of propellant. In this work, I_{sp} is obtained by

$$I_{sp} = \frac{I_{total}}{mg} \tag{1}$$

where I_{total} is the sum of all impulse bit measurements for a given trial and g is the acceleration due to gravity. In a previous work, the ablation mass m was investigated in a similar device [26]. The same propellant sample preparation procedures were followed in this work, and similar mass losses were measured during short duration tests. In general, ablation mass increases in a linear fashion as a function of discharge energy. For PTFE, the ablation mass at 5 J is 35.3 μg/pulse which yields a specific ablation of ~7 μg/J. For the other, higher energy levels, the specific ablation is on average a constant ~6.3 μg/J. HIPEP ablation exhibits similar scaling, but at a specific ablation rate that is much greater than PTFE. At 5 J, the ablation mass of HIPEP is on average 106.8 μg/pulse or ~21 μg/J, which is about three times that of PTFE. The specific ablation of HIPEP decreases to about 12.5 μg/J at the higher discharge energy levels tested. This is roughly twice that of PTFE. Because the measured impulse bits at all energy levels are nearly identical between the two propellants, the higher mass ablated per pulse results in a specific impulse for HIPEP that is significantly lower than for PTFE. The I_{sp} of both propellants were calculated using Eq. (1) for the short-duration (100 pulse) test trials and the results are presented in Figure 8. The measurement error for HIPEP (ϵ_H) specific impulse is ±50 s based on mass loss measurement error of ±35 μg/pulse [26] and impulse measurement error of ±20 μN-s. For PTFE, the measurement error (ϵ_P) is ±30 s. These errors are shown as representative error bars in Figure 8.

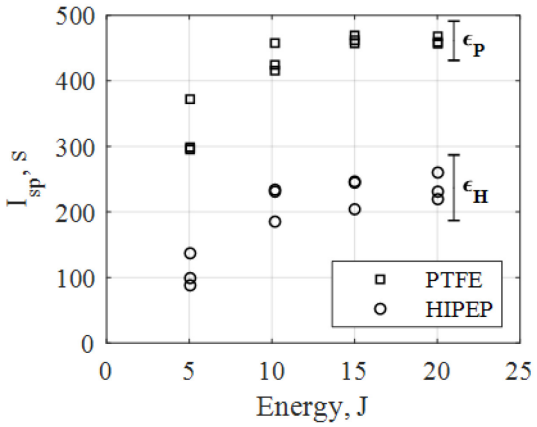

Figure 8: Specific impulse as a function of energy for each short-duration test for each propellant. Representative error bars are shown for HIPEP (ϵ_H) and PTFE (ϵ_P).

Because of the increased ablation mass relative to stored energy, the specific impulse at 5 J is reduced for both propellants. For PTFE, the average I_{sp} at 5 J is ~320 s compared to >400 s at the higher energy levels. HIPEP specific impulse at 5 J is on average ~100 s, but is typically above 200 s at 10, 15, and 20 J. The reduced specific impulse at 5 J relative to a mostly constant value for other energies indicates this device may be operating in a different mode at low energy. One option is that a charring phenomenon observed in APPTs using PTFE as propellant at low energy is reducing the specific impulse. In the case of current density over the propellant surface below some threshold, excessive carbonization (i.e. charring) of the PTFE occurs and leads to non-uniform ablation [31, 32]. It is possible that this non-uniformity may translate to non-uniform heating of the ablated material and thus a lower average exhaust velocity and specific impulse. Alternatively, at the low energy level, the energy available for the arc discharge may be too low to sustain a breakdown across the entire gap, yielding an incomplete current channel that can not dissipate the electrical energy efficiently. Though the EPTX device is not optimized as a thruster, its performance is near to that of other similar devices. The measured I_{sp} for PTFE at 10 J or above in this work is comparable to other coaxial geometry APPTs using PTFE as propellant. For example, the IL (University of Illinois) coaxial PPT was measured

to have specific impulse of 500-600 s operating with a stored energy of 7.5 J/pulse [10, 29]. Various configurations of the ablative Z-pinch PPT, which possesses a geometry similar to the EPTX, exhibited specific impulse in the range of ~300-600 s [19]. On average, over the three higher energy levels, the specific impulse for PTFE is calculated to be ~450 s, compared to ~225 s for HIPEP. The measured impulse bits between propellants was virtually identical but the ablation mass for HIPEP was significantly greater. This leads to the conclusion that much of the additional mass ablated when operating on HIPEP did not appreciably contribute to increasing the impulse bit, but rather that it was expelled at a low average velocity. This may be due to one or both of the following phenomena. Additional mass ablated while operating on HIPEP could require significantly more energy to heat to a temperature required to achieve an exhaust velocity similar to PTFE. Or a large portion of the additional mass ablated could be liberated after the discharge is complete (late time ablation), ejected in the form of low speed vapor and macroparticles that generate little to no additional contribution to the impulse bit. Evidence of late time ablation for HIPEP has been confirmed but not thoroughly quantified in a previous work [28, 33].

B. Propellant Sample Lifetime

The main driving factor in end-of-life for this device configuration is the ratio of stored electrical energy to exposed propellant surface area, or the energy density (J/mm^2). At beginning-of-life, the propellant sample inner diameter is the nominal 6.35 mm and energy density is at a maximum. Each pulse of the device ablates a portion of the inner wall of the propellant cavity, increasing the inner diameter and exposed propellant surface area. Assuming that this ablation occurs uniformly along the azimuthal and axial directions, the final diameter, d_2 may be determined by

$$d_2 = \sqrt{d_1^2 + \frac{4m}{\pi\rho l}} \tag{2}$$

where d_1 is the initial inner diameter of the propellant sample, l is the sample length, ρ is the density of the propellant, and m is the total mass loss over the course of the test trial. Comparison of d_2 calculated by Eq. (2) with measured inner diameter showed excellent agreement to within 0.2 mm for PTFE. Measurements for inner diameter of HIPEP samples were complicated by the flexibility of the material, but predictions for d_2 are typically 1-10% greater than for PTFE due to the increased HIPEP mass loss, m, and lower HIPEP density, ρ. The ratio of stored energy to propellant surface area reaches a minimum threshold at end-of-life, making the ignition of a discharge difficult or impossible. Based on calculations and measurements of PTFE sample inner diameters, the threshold for this behavior is 20-60 mJ/mm^2. The threshold for HIPEP is similar. Based on the predicted value of d_2 the threshold is 20-50 mJ/mm^2. The specific value of the energy density threshold described here is likely dependent on the energy of the igniter used to trigger the arc discharge and the overall geometry of the setup. In the present work, the igniter has a stored energy of ~40 mJ and is not adjustable. Future designs utilizing HIPEP as propellant in an APPT are likely to use a similar method and must be designed to expend all propellant before reaching the threshold for igniting a discharge.

In Figure 6, a clear distinction in test duration is observed between propellants. Long-duration tests with PTFE at each energy level yielded more total pulses than for each test with HIPEP. For instance, at 5 J, the end-of-life for a HIPEP sample occurred after 793 pulses, only 39% of the 2,000 pulses for a sample of PTFE. While this is the largest difference in the testing performed, the HIPEP lifetime at 10 and 15 J is only 43% and 86% of PTFE, respectively. The difference in lifetime is caused by two major differences in the propellant materials. First, the density of HIPEP is only 1.8 g/cm^3 compared to 2.2 g/cm^3 for PTFE. Thus, even for constant propellant consumption rate (i.e., equal µg/pulse) between propellants, the change in inner diameter would still be greater for HIPEP. Second, as discussed in section IV.A, at a given energy the ablation rate for HIPEP is typically twice that of PTFE. Together, the higher ablation rate and lower propellant density of HIPEP serve to significantly reduce that propellant's overall lifetime relative to PTFE.

V. Conclusions

A compact thrust stand of inverted pendulum design was used to measure the impulse of an electrothermal APPT. This device was operated using both PTFE and an electric solid propellant, HIPEP, as propellant. The impulse bit for PTFE was around 100 µN-s for 5 J of initial stored energy and it increased by ~30 µN-s per Joule of additional stored energy. The impulse bit for HIPEP was typically 95-99% of PTFE, exhibiting similar trends at each of the four energy levels tested (5, 10, 15, and 20 J). The device used in this work was not designed as an optimized APPT, so the specific impulse for PTFE is roughly 450 s. This is just at the bottom of the range of other coaxial APPTs tested using PTFE. The ablated mass of HIPEP for a given discharge energy is typically double that of PTFE and, as a result, the calculated specific impulse is approximately half that of the thruster operating on PTFE. In the present work, we have found that the additional ablated mass does not increase the measured impulse when compared with the thruster

operating on PTFE under identical testing conditions. These new insights and combined understanding of the propellant ablation, thermochemistry, and propulsion performance can help guide future design of pulsed electric devices using this propellant. In the early pulses of a test (< 10 pulses), impulse measurements are typically up to 30% greater than the mean impulse. Though the additional total impulse imparted during this region of test is not significant, it is unclear how much propellant mass is expelled during these early pulses. For the hygroscopic HIPEP material, it could be an amount of absorbed moisture is evaporated during these pulses due to high transient heating. This evaporation could skew mass loss measurements, and potentially bias calculated specific impulse.

Acknowledgments

M.S. Glascock would like to graciously thank the NASA Space Technology Research Fellowship program for funding his graduate research via grant NNX15AP31H. This work is a large part of that research and would not be possible without the support from this program. Additionally, the authors wish to thank DSSP for providing the HIPEP material in custom-made form for our research, as well as numerous discussions on the nuances of HIPEP operation and handling.

References

[1] Sawka, W. N., and McPherson, M., "Electrical Solid Propellants: A Safe, Micro to Macro Propulsion Technology," *49th Joint Propulsion Conference*, AIAA Paper 2013-4168, San Jose, CA, 2013.
doi:10.2514/6.2013-4168

[2] Sawka, W. N., U.S. Patent for a "Controllable Digital Solid State Cluster Thrusters for Rocket Propulsion and Gas Generation," No. 7958823 B2 and 8464640; June 14, 2011 and June 18, 2013.

[3] Dulligan, M., U.S. Patent for a "Electrically Controlled Extinguishable Solid Propellant Motors," No. 7788900B2; September 7, 2010.

[4] Chung, K., Rozumov, E., Kaminsky, D., Buescher, T., Manship, T., Valdivia, A., Cook, P., and Anderson, P., "Development of Electrically Controlled Energetic Materials," *ECS Transactions,* Vol. 50, No. 40, 2013, pp. 59-66.
doi: 10.1149/05040.0059ecst

[5] Grix, C., and Sawka, W. N., U.S. Patent for a "Family of Modifiable High Performance Electrically Controlled Propellants and Explosives," No. 8888935B2; November 18, 2011.

[6] Sawka, W. N., and Grix, C., U.S. Patent for a "Family of Metastable Intermolecular Composites Utilizing Energetic Liquid Oxidizers with Nanoparticle Fuels in Sol-Gel Polymer Network," No. 8317953B2; November 27.

[7] Baird, J. K., Lang, J. R., Hiatt, A. T., and Frederick, R. A., "Electrolytic Combustion in the Polyvinyl Alcohol Plus Hydroxylammonium Nitrate Solid Propellant," *Journal of Propulsion and Power,* Vol. 33, No. 6, 2017, pp. 1589-1590.
doi: 10.2514/1.B36450

[8] Hiatt, A. T., and Frederick, R. A., "Laboratory Experimentation and Basic Research Investigation Electric Solid Propellant Electrolytic Characteristics," *52nd AIAA/SAE/ASEE Joint Propulsion Conference*, AIAA Paper 2016-4935, Salt Lake City, UT, 2016.
doi:10.2514/6.2016-4935

[9] Sawka, W. N., and Grix, C., U.S. Patent for a "Electrode Ignition and Control of Electrically Ignitable Materials," No. 8857338B2; October 14.

[10] Burton, R. L., and Turchi, P. J., "Pulsed Plasma Thruster," *Journal of Propulsion and Power,* Vol. 14, No. 5, 1998, pp. 716-735.
doi: 10.2514/2.5334

[11] Gatsonis, N. A., Lu, Y., Blandino, J., Demetriou, M. A., and Paschalidis, N., "Micropulsed Plasma Thrusters for Attitude Control of a Low-Earth-Orbiting CubeSat," *Journal of Spacecraft and Rockets,* Vol. 53, No. 1, 2016, pp. 57-73.
doi: 10.2514/1.A33345

[12] Keidar, M., Zhuang, T., Shashurin, A., Teel, G., Chiu, D., Lukas, J., Haque, S., and Brieda, L., "Electric Propulsion for Small Satellites," *Plasma Physics and Controlled Fusion,* Vol. 57, No. 1, 2015, pp. 1-10.
doi: 10.1088/0741-3335/57/1/014005

[13] Bushman, S., and Burton, R. L., "Heating and Plasma Properties in a Coaxial Gasdynamic Pulsed Plasma Thruster," *Journal of Propulsion and Power,* Vol. 17, No. 5, 2001, pp. 959-966.
doi: 10.2514/2.5849

[14] Cheng, L., Wang, Y., Ding, W., Ge, C., Yan, J., Li, Y., Li, Z., and Sun, A., "Experimental Study on the Discharge Ignition in a Capillary Discharge Based Pulsed Plasma Thruster," *Physics of Plasma,* Vol. 25, No. 9, 2018.
doi: 10.1063/1.5038087

[15] Wang, Y., Ding, W., Cheng, L., Yan, J., Li, Z., Wang, J., and Wang, Y., "An Investigation of Discharge Characteristics of an Electrothermal Pulsed Plasma Thruster," *IEEE Transactions on Plasma Science,* Vol. 45, No. 10, 2017, pp. 2715-2724.
doi: 10.1109/TPS.2017.2738330

[16] al., A. e., "Total Impulse Improvement of Coaxial Pulsed Plasma Thruster for Small Satellite," *Vacuum,* Vol. 83, No. 1, 2008, pp. 72-76.

doi: 10.1016/j.vacuum.2008.03.082
[17] Edamitsu, T., and Tahara, H., "Experimental and Numerical Study of an Electrothermal Pulsed Plasma Thruster for Small Satellites," *Vacuum,* Vol. 80, No. 11, 2006, pp. 1223-1228.
doi: 10.1016/j.vacuum.2006.01.055
[18] Miyasaka, T., Asato, K., Sakaguchi, N., and Ito, K., "Optical Measurements of Unsteady Phenomena on Coaxial Pulsed Plasma Thrusters," *Vacuum,* Vol. 88, 2013, pp. 52-57.
doi: 10.1016/j.vacuum.2012.04.003
[19] Markusic, T. E., Polzin, K. A., Choueiri, E. Y., Keidar, M., Boyd, I. D., and Lepsetz, N., "Ablative Z-Pinch Pulsed Plasma Thruster," *Journal of Propulsion and Power,* Vol. 21, No. 3, 2005, pp. 392-400.
doi: 10.2514/1.4362
[20] Keidar, M., Boyd, I. D., and Beilis, I. I., "Electrical Discharge in the Teflon Cavity of a Coaxial Pulsed Plasma Thruster," *IEEE Transactions on Plasma Science,* Vol. 28, No. 2, 2000, pp. 376-385.
doi: 10.1109/27.848096
[21] Keidar, M., Boyd, I. D., and Beilis, I. I., "Model of an Electrothermal Pulsed Plasma Thruster," *Journal of Propulsion and Power,* Vol. 19, No. 3, 2003, pp. 424-430.
doi: 10.2514/2.6125
[22] Ruchti, C. B., and Niemeyer, L., "Ablation Controlled Arcs," *IEEE Transactions on Plasma Science,* Vol. PS-14, No. 4, 1986, pp. 423-434.
doi: 10.1109/TPS.1986.4316570
[23] Schönherr, T., Komurasaki, K., and Herdrich, G., "Propellant Utilization Efficiency in a Pulsed Plasma Thruster," *Journal of Propulsion and Power,* Vol. 29, No. 6, 2013, pp. 1478-1487.
doi: 10.2514/1.B34789
[24] Seeger, M., Tepper, J., Christen, T., and Abrahamson, J., "Experimental Study on PTFE Ablation in High Voltage Circuit-Breakers," *Journal of Physics D: Applied Physics,* Vol. 39, No. 23, 2006, pp. 5016-5024.
doi: 10.1088/0022-3727/39/23/018
[25] Wang, W., Kong, L., Geng, J., Wei, F., and Xia, G., "Wall Ablation of Heated Compound-Materials into Non-Equilibrium Discharge Plasmas," *Journal of Physics D: Applied Physics,* Vol. 50, No. 7, 2017.
doi: 10.1088/1361-6463/aa5606
[26] Glascock, M. S., Rovey, J. L., and Polzin, K. A., "Electric Solid Propellant Ablation in an Arc Discharge," *Journal of Propulsion and Power*, 2019, pp. 1-10, Online July 2019.
doi: 10.2514/1.B37517
[27] Glascock, M. S., Rovey, J. L., Williams, S., and Thrasher, J., "Plume Characterization of Electric Solid Propellant Pulsed Microthrusters," *Journal of Propulsion and Power,* Vol. 33, No. 4, 2017, pp. 870-880.
doi: 10.2514/1.B36271
[28] Glascock, M. S., "Characterization of Electric Solid Propellant Pulsed Microthrusters," M.S. Thesis, Missouri University of Science and Technology, 2016.
[29] Wilson, M. J., Bushman, S., and Burton, R. L., "A Compact Thrust Stand for Pulsed Plasma Thrusters," *25th International Electric Propulsion Conference*, ERPS Paper IEPC-97-122, Cleveland, OH, 1997.
[30] Polk, J. E., Pancotti, A., Haag, T., King, S., Walker, M. L. R., Blakely, J., and Ziemer, J., "Recommended Practice for Thrust Measurement in Electric Propulsion Testing," *Journal of Propulsion and Power,* Vol. 33, No. 3, 2017, pp. 539-555.
doi: 10.2514/1.B35564
[31] Keidar, M., Boyd, I. D., Antonsen, E. L., Burton, R. L., and Spanjers, G. G., "Optimization Issues for a Micropulsed Plasma Thruster," *Journal of Propulsion and Power,* Vol. 22, No. 1, 2006, pp. 48-55.
doi: 10.2514/1.13954
[32] Keidar, M., Boyd, I. D., Antonsen, E. L., Gulczinski III, F. S., and Spanjers, G. G., "Propellant Charring in Pulsed Plasma Thrusters," *Journal of Propulsion and Power,* Vol. 20, No. 6, 2004, pp. 978-984.
doi: 10.2514/1.2471
[33] Glascock, M. S., Rovey, J. L., Williams, S., and Thrasher, J., "Observation of Late-Time Ablation in Electric Solid Propellant Pulsed Microthrusters," *52nd AIAA/SAE/ASEE Joint Propulsion Conference*, AIAA Paper 2016-4845, Salt Lake City, UT, 2016.
doi:10.2514/6.2016-4845